Dynamics of a ring-laser gyroscope with backscattering

C. Etrich and Paul Mandel
Université Libre de Bruxelles, Campus Plaine, Code Postal 231, 1050 Bruxelles, Belgium

R. Centeno Neelen, R. J. C. Spreeuw, and J. P. Woerdman
Huygens Laboratory, University of Leiden, P.O. Box 9504, 2300 RA Leiden, The Netherlands
(Received 3 December 1991)

We analyze the standard third-order model describing a laser gyroscope with backscattering in the two limiting cases of dissipative and conservative coupling. In both cases we discuss the steady-state and periodic solutions, determine their stability, and construct the locking diagram. In particular, in the dissipative coupling case, an exact periodic solution is found analytically. It is also proved that the concepts developed in the passive-cavity problem are useful tools to understand the dynamics of the laser gyroscope.

PACS number(s): 42.60.−v, 42.65.−k

I. INTRODUCTION

The behavior of the counterpropagating traveling waves in a ring laser in the presence of backscattering has been intensively studied during the past two decades [1–14]. The backscattering produces a linear coupling of the two counterpropagating waves. It can lead to locking phenomena if the ring laser is used as a gyroscope [1–7], or more generally modify the intensity correlations of the counterpropagating beams [8–14]. In particular it can lead to so-called oscillatory instabilities [2,7,11,13,14] or intensity oscillations and phase jumps [10,11,13]. An alternative approach towards mode coupling in bidirectional ring lasers can be found in [15].

In this paper we want to discuss the locking behavior of two-mode ring-laser gyroscopes induced by backscattering. The full analysis of such systems as presented here substantiates the assumption that many of their features can be related to the mode structure of the passive rotating ring cavity [15]. For instance, depending on the nature of the backscattering, the mode structure of the passive rotating ring cavity displays either frequency locking or frequency repulsion. This distinction leads to different locking behaviors in the active ring-laser gyroscope. Two limiting cases, referred to as the dissipatively and conservatively coupled ring-laser gyroscopes, are discussed and the locking diagrams for both are shown to be completely different. Theoretical discussions of locking in laser gyroscopes so far have been mainly restricted to the dissipative case.

The paper is organized as follows. In Sec. II we present the theoretical model describing the ring-laser gyroscope. In Sec. III we focus on the case of dissipative coupling and discuss steady-state and periodic solutions as well as their stability properties analytically. This leads to the locking behavior of the ring-laser gyroscope. Section IV deals with the case of conservative coupling. Again steady-state and periodic solutions with their stability properties are discussed, leading to a fundamentally different locking behavior compared with the dissipative coupling case. Finally the results are summarized in Sec. V.

II. THE THEORETICAL MODEL

The starting points of our analysis are the standard dimensionless third-order nonlinear evolution equations for the counterpropagating complex electric fields $\tilde{E}_1$ and $\tilde{E}_2$ in a rotating ring laser with backscattering:

$$\partial_t \tilde{E}_1 = (a - |\tilde{E}_1|^2 - \xi|\tilde{E}_2|^2)\tilde{E}_1 - iVe^{i\phi}\tilde{E}_2 - i\Omega\tilde{E}_1 , \quad (2.1a)$$

$$\partial_t \tilde{E}_2 = (a - |\tilde{E}_2|^2 - \xi|\tilde{E}_1|^2)\tilde{E}_2 - iVe^{i\phi}\tilde{E}_1 + i\Omega\tilde{E}_2 . \quad (2.1b)$$

Here a is the pump parameter and ξ is the mode-coupling parameter determining the strength of the nonlinear coupling of the modes defined as the ratio of the cross saturation and the self-saturation. Expressions for these parameters can be found in [3,16]. In general, we consider the so-called weak coupling case $0<\xi<1$, corresponding, for instance, to the conventional He-Ne laser gyroscope tuned off line center. The limit of neutral coupling, $\xi=1$, corresponding, for instance, to a He-Ne laser gyroscope with a single Ne isotope tuned to line center, is studied extensively in the literature [9,12,13] and is addressed only briefly here. The strength of the linear coupling (or backscattering rate) $V>0$ is proportional to the fractional amount of backscattering per round-trip. The rotation rate is Ω. The value of the phase ϕ determines the nature of the backscattering. We consider the two limiting cases $\phi=\pi(2k+1)/2$ and $\phi=k\pi$, with integer k, referred to as dissipative (or in-phase) and conservative (or off-phase) coupling, respectively [8].

Introducing the polar decomposition of the fields, i.e.,

$$\tilde{E}_j = E_j \exp[-i(\mu_j + \omega t)] , \quad (2.2)$$

and separating real and imaginary parts, Eqs. (2.1) become

$$\partial_t E_1 = (a - E_1^2 - \xi E_2^2)E_1 + VE_2 \sin(\mu+\phi) , \quad (2.3a)$$

$$\partial_t E_2 = (a - E_2^2 - \xi E_1^2)E_2 - VE_1 \sin(\mu-\phi) , \quad (2.3b)$$

$$\partial_t \mu = V[E_2^2\cos(\mu+\phi)-E_1^2\cos(\mu-\phi)]\frac{1}{E_1E_2}+2\Omega \ , \tag{2.3c}$$

with $\mu=\mu_1-\mu_2$ and the phase equations

$$E_1\partial_t\mu_1 = VE_2\cos(\mu+\phi)+\Omega E_1-\omega E_1 \ , \tag{2.4a}$$

$$E_2\partial_t\mu_2 = VE_1\cos(\mu-\phi)-\Omega E_2-\omega E_2 \ , \tag{2.4b}$$

showing that one of the phases is only determined up to a constant.

Equations (2.1) admit the trivial solution $\tilde{E}_1=\tilde{E}_2=0$. To determine the stability of this solution, we substitute $\tilde{E}_j=\epsilon\zeta_j(t)$ with $0<\epsilon\ll 1$ into Eqs. (2.1) and linearize with respect to ϵ:

$$\partial_t\zeta_1 = a\zeta_1 - iVe^{i\phi}\zeta_2 - i\Omega\zeta_1 \ , \tag{2.5a}$$

$$\partial_t\zeta_2 = a\zeta_2 - iVe^{i\phi}\zeta_1 + i\Omega\zeta_2 \ . \tag{2.5b}$$

The time dependence of $\zeta_j(t)$ is governed by the roots of a characteristic equation which is easily solved to yield

$$\begin{aligned} &\lambda_1 = a+(-V^2e^{2i\phi}-\Omega^2)^{1/2}, \quad \lambda_2=\lambda_1^* \ , \\ &\lambda_3 = a-(-V^2e^{2i\phi}-\Omega^2)^{1/2}, \quad \lambda_4=\lambda_3^* \ . \end{aligned} \tag{2.6}$$

For dissipative coupling, $\phi=\pi(2k+1)/2$, the four roots are

$$\lambda_j = a\pm(V^2-\Omega^2)^{1/2}, \quad \Omega<V \ , \tag{2.7a}$$

$$\lambda_j = a\pm i(\Omega^2-V^2)^{1/2}, \quad \Omega>V \ . \tag{2.7b}$$

Hence there is a degenerate steady bifurcation ($\lambda=0$ is a double root) at $a=\pm(V^2-\Omega^2)^{1/2}$ for $\Omega<V$ and a degenerate Hopf bifurcation (λ purely imaginary) at $a=0$ for $\Omega>V$. Hence the lasing first threshold is $a_{\rm th}=-(V^2-\Omega^2)^{1/2}$ for $\Omega<V$ and $a_{\rm th}=0$ for $\Omega>V$.

For conservative coupling, $\phi=\pi k$, we have a pair of doubly degenerate roots

$$\lambda_j = a\pm i(\Omega^2+V^2)^{1/2} \ , \tag{2.8}$$

and therefore a degenerate Hopf bifurcation at $a_{\rm th}=0$.

Note that if there is no net gain, i.e., for $a=0$, Eqs. (2.5) describe the passive-cavity case which has been discussed in detail in [15]. In this paper we focus our attention on the lasing domain, corresponding to the inequality $a>a_{\rm th}$.

III. DISSIPATIVE COUPLING

A. Steady-state solutions and their stability

In this section, we analyze the nontrivial steady-state solutions of Eqs. (2.3) and (2.4) for dissipative coupling and determine their stability. The steady-state equations are

$$(a-E_1^2-\xi E_2^2)E_1+VE_2\cos(\mu)=0 \ , \tag{3.1a}$$

$$(a-E_2^2-\xi E_1^2)E_2+VE_1\cos(\mu)=0 \ , \tag{3.1b}$$

$$V(E_1^2+E_2^2)\sin(\mu)-2\Omega E_1E_2=0 \ , \tag{3.1c}$$

$$V(E_1^2-E_2^2)\sin(\mu)-2\omega E_1E_2=0 \ . \tag{3.1d}$$

Equations (3.1c) and (3.1d) determine the frequency ω:

$$\omega=\Omega\frac{E_1^2-E_2^2}{E_1^2+E_2^2} \ . \tag{3.2}$$

From the two amplitude equations, Eqs. (3.1a) and (3.1b), we derive the relation

$$(E_1^2+E_2^2-a)(E_1^2-E_2^2)=0 \ , \tag{3.3}$$

which admits two solutions, either $E_{10}=E_{20}$ or $E_{10}^2+E_{20}^2=a$.

(1) The solution $E_{10}=E_{20}$ implies $\omega=0$. The intensity and the phase difference are given by

$$\begin{aligned} &E_{10}^2=\frac{a+V\cos(\mu_0)}{1+\xi}, \quad \sin(\mu_0)=\frac{\Omega}{V} \ , \\ &\cos(\mu_0)=\pm(1-\Omega^2/V^2)^{1/2} \ . \end{aligned} \tag{3.4}$$

The existence of these solutions requires that $\Omega<V$; then $\cos(\mu_0)$ has two determinations, corresponding to two branches that bifurcate at $a=\mp(V^2-\Omega^2)^{1/2}$ from the trivial solution.

(2) The solution with $E_{10}^2+E_{20}^2=a$ has a markedly different behavior because $\omega\neq 0$. The intensities and the phase difference are given by

$$\begin{aligned} &E_{10}^2=\frac{a}{2}\left\{1\pm\left[\frac{a^2(1-\xi)^2-4(V^2-\Omega^2)}{a^2(1-\xi)^2+4\Omega^2}\right]^{1/2}\right\} \ , \\ &E_{20}^2=a-E_{10}^2 \ , \\ &\tan(\mu_0)=-\frac{2\Omega}{a(1-\xi)} \ , \end{aligned} \tag{3.5}$$

where $\pi/2\le\mu_0\le\pi$. Two cases have to be considered. (i) For $\Omega<V$ these solutions exist for $a^2(1-\xi)^2>4(V^2-\Omega^2)$ and oscillate harmonically with frequencies $\pm\omega$. They are still referred to as steady-state solutions because the corresponding intensities E_{10}^2 and E_{20}^2 are time independent. These solutions do not exist if $\xi=1$. (ii) For $\Omega>V$ the steady-state solutions (3.5) bifurcate at $a=0$ from the trivial solution, the frequency ω being equal to the frequency of the Hopf bifurcation at this point.

The stability of the steady-state solutions (3.4) and (3.5) is governed by the eigenvalues of the Jacobian of Eqs. (2.3). Linearizing Eqs. (2.3) around a given solution E_{10}, E_{20}, and μ_0, the Jacobian is

$$J=\begin{bmatrix} a-3E_{10}^2-\xi E_{20}^2 & -2\xi E_{10}E_{20}+V\cos(\mu_0) & -VE_{20}\sin(\mu_0) \\ -2\xi E_{10}E_{20}+V\cos(\mu_0) & a-3E_{20}^2-\xi E_{10}^2 & -VE_{10}\sin(\mu_0) \\ -V\left[\dfrac{E_{10}^2-E_{20}^2}{E_{10}^2E_{20}}\right]\sin(\mu_0) & V\left[\dfrac{E_{10}^2-E_{20}^2}{E_{10}E_{20}^2}\right]\sin(\mu_0) & -V\left[\dfrac{E_{10}^2+E_{20}^2}{E_{10}E_{20}}\right]\cos(\mu_0) \end{bmatrix} . \tag{3.6}$$

Substituting the solution (3.4) into Eq. (3.6), the eigenvalues of the Jacobian are found to be

$$\lambda_1=-2[2V\cos(\mu_0)+a(1-\xi)]/(1+\xi),\quad \lambda_2=-2[a+V\cos(\mu_0)],\quad \lambda_3=-2V\cos(\mu_0)\ . \tag{3.7}$$

It follows that the branch with $\cos(\mu_0)>0$ is always stable and the branch with $\cos(\mu_0)<0$ always unstable. At $a(1-\xi)=-2V\cos(\mu_0)$ we have $\lambda_1=0$ if $\cos(\mu_0)<0$. From this point on the unstable branch of solutions (3.4), the branches of solutions (3.5) bifurcate. Substituting these solutions into Eq. (3.6) the characteristic equation is

$$\lambda^3+2a\xi\lambda^2-\{a^2(1-\xi^2)+[2(1-\xi)-4\Omega^2/a^2](E_{10}^2-E_{20}^2)^2\}\lambda+\frac{2}{a}[a^2(1-\xi)^2+4\Omega^2](E_{10}^2-E_{20}^2)^2=0\ . \tag{3.8}$$

Since the constant term of this polynomial is always different from zero (except at the bifurcation where $E_{10}=E_{20}$) there are no steady bifurcations on this branch. The condition for a Hopf bifurcation can be derived as

$$a^2\xi(1+\xi)+(1+\xi+4\Omega^2/a^2)(E_{10}^2-E_{20}^2)^2=0\ . \tag{3.9}$$

Since the left-hand side of this equation is always positive there are no Hopf bifurcations on this branch.

In conclusion, for $\Omega<V$ this branch bifurcates unstably and remains unstable. For $\Omega>V$ an expansion in powers of a yields for the roots of the characteristic equation (3.8) $\lambda_1=-2a+\mathcal{O}(a^2)$ and $\lambda_{2,3}=\pm i2(\Omega^2-V^2)^{1/2}+a(1-\xi)+\mathcal{O}(a^2)$. This shows that the branches of solutions (3.5) bifurcate unstably from the trivial solution, except if $\xi=1$. In this case the expansion up to $\mathcal{O}(a)$ is exact and the solution is a continuum of marginally stable points since $\mathrm{Re}(\lambda_{2,3})=0$.

B. Periodic solutions and their stability

In the preceding section we found that there are no stable steady-state solutions for $\Omega>V$, except for the limiting case $\xi=1$. Instead, let us show that there is a branch of stable periodic solutions with $E_1(t)=E_2(t)=E(t)$. For solutions fulfilling this condition, Eqs. (2.3) reduce to

$$\partial_t I=2I[a-(1+\xi)I+V\cos(\mu)]\ , \tag{3.10a}$$

$$\partial_t\mu=-2V\sin(\mu)+2\Omega\ , \tag{3.10b}$$

where $I=E^2$ has been used. Note that Eq. (3.10b) is the conventional locking equation, from which the phase difference is obtained as

$$\tan\left[\frac{\mu(t)}{2}\right]=\frac{1}{\Omega}[V+\omega_0\tan(\omega_0 t+\varphi_0)]\ , \tag{3.11}$$

where $\omega_0=(\Omega^2-V^2)^{1/2}$ and φ_0 is an arbitrary constant. The expression for the phase difference can be substituted into Eq. (3.10a). By means of the nonlinear transformation $I=a/[1+\xi+C(t)\exp(-2at)]$, this equation becomes a linear equation for $C(t)$:

$$\frac{dC}{dt}=-2V\cos(\mu)[C+(1+\xi)e^{2at}]\ , \tag{3.12}$$

which is easily solved, and $I(t)$ becomes

$$I(t)=E^2(t)=\frac{a(a^2+\omega_0^2)^{1/2}[\Omega+V\cos(2\omega_0 t-\varphi_1)]}{(1+\xi)[\Omega(a^2+\omega_0^2)^{1/2}+aV\cos(2\omega_0 t-\varphi_2)]}\ , \tag{3.13}$$

where we set $\varphi_0=0$. The constants φ_1 and φ_2 are defined via

$$\tan(\varphi_1)=\frac{\omega_0}{V},\quad \tan(\varphi_2)=\frac{\omega_0(a+V)}{aV-\omega_0^2}\ , \tag{3.14}$$

where $0\le\varphi_j\le\pi$, $j=1,2$. The periodic solution defined by Eqs. (3.11) and (3.13) exists for $a>0$ and $\Omega>V$, and oscillates with a frequency independent of a. In terms of the pump parameter a, it bifurcates at $a=0$ from the trivial solution, together with the steady-state solution (3.5). In terms of Ω, the two branches of the steady-state solution (3.4) coincide at $\Omega=V$. This limit point can be considered as a degenerate Hopf bifurcation with zero frequency from which the branch of periodic solutions emerges. At this point all three branches coincide with $I=a/(1+\xi)$. Away from this point the periodic solutions oscillate with a finite amplitude (Fig. 1). Note that the solutions (3.11) and (3.13) can be analytically continued into the domain $\Omega<V$. Indeed, using $\omega_0=i(V^2-\Omega^2)^{1/2}$, the functions (3.11) and (3.13) approach the stable branch of solutions (3.4) in the long-time limit.

To analyze the stability of the branch of periodic solutions, we substitute in the Jacobian (3.6) E_{10} and E_{20} by $E(t)$, and μ_0 by $\mu(t)$, where $E(t)$ and $\mu(t)$ are given by Eqs. (3.11) and (3.13). In this way we find that the branch of periodic solutions is linearly stable in the domain in parameter space where it exists. The explicit calculation of this stability analysis is presented in Appendix A.

To compare with the limiting case $\xi=1$, we derive the long-time limit of the general solution of Eqs. (2.1) for $\Omega>V$, using a similar transformation as in [13]. The field amplitudes $E_j(t)$ and the phase difference $\mu(t)$ are

$$E_{1,2}^2(t)=\frac{a(a^2+\omega_0^2)^{1/2}[\Omega(1+R^2)\pm\omega_0(1-R^2)+2RV\cos(2\omega_0 t-\varphi_1)]}{2[(1+R^2)\Omega(a^2+\omega_0^2)^{1/2}+2RaV\cos(2\omega_0 t-\varphi_2)]}\ , \tag{3.15a}$$

$$\tan[\mu(t)]=\frac{2(1/\Omega)[V+\omega_0\tan(\omega_0 t)]+[V(1-R)^2/2\Omega R][1+\tan^2(\omega_0 t)]}{1-\{(1/\Omega)[V+\omega_0\tan(\omega_0 t)]\}^2}\ , \tag{3.15b}$$

where R is a constant parametrizing the family of solutions. If $R=1$, we recover the solutions (3.11) and (3.13) with $\xi=1$. The steady-state solution (3.5) corresponds to $R=0$ or $R\to\infty$.

To sum up the results of the previous two sections, the laser behavior, as the pump parameter a increases above threshold, is characterized by a constant output intensity for $\Omega<V$, and by a periodically modulated output intensity for $\Omega>V$.

C. Locking behavior

The locking behavior of the ring-laser gyroscope is best discussed by means of a so-called locking diagram. Such a diagram displays the beat frequency as a function of the rotation rate Ω. The beat frequency is defined as the average time derivative of the phase difference μ:

$$\langle\partial_t\mu\rangle=\frac{1}{T}\int_0^T dt\,\partial_t\mu\ , \tag{3.16}$$

where T is the period of $\mu(t)$. In the range $0<\Omega<V$, there is a stable steady state and $\langle\partial_t\mu\rangle=0$. The laser gyroscope is said to be locked for this regime. For $\Omega>V$ there is a stable periodic solution (Fig. 1). Using Eq. (3.11), the beat frequency is

$$\langle\partial_t\mu\rangle=2\omega_0=2(\Omega^2-V^2)^{1/2}\ . \tag{3.17}$$

Hence the locking range is given by $\Omega_{L,d}=V$ which is independent of the pump parameter a (Fig. 2). For $\Omega\gg\Omega_{L,d}$ we recover the behavior of an ideal ring-laser gyroscope, as can also be seen from Eqs. (3.11) and (3.13). In this limit, the phase difference approaches $\mu(t)=2\omega_0 t=2\Omega t$, leading to an observed beat frequency which is linear in Ω (Fig. 2).

Comparing the above results with the passive-cavity case, which is essentially described by Eqs. (2.5) with $a=0$ and $\phi=\pi(2k+1)/2$, we see that both the locking range and the locking diagram are the same [15]. Locking occurs in the passive-cavity case since the eigenmodes of Eqs. (2.5) are damped for $\Omega<V$. For $\Omega>V$ the eigenmodes are harmonically oscillating with frequencies $\pm\omega_0$ and the so-called Sagnac beat frequency can be observed.

IV. CONSERVATIVE COUPLING

A. The case $a\ll 1$

For conservative coupling, the trivial solution becomes unstable via a Hopf bifurcation at $a=0$. As in the case of dissipative coupling for $\Omega>V$, we expect that a branch of harmonically oscillating solutions (with steady-state intensity) and a branch of periodic solutions (with oscillating intensity) bifurcate from this point. To show this and to make the connection to the passive-cavity case, we perform a local analysis in the vicinity of $a=0$. Our starting point is the system of Eqs. (2.1), and we seek solutions of the form

$$\tilde{E}_1(\tau,t)=\varepsilon\tilde{E}_{11}(\tau,t)+\varepsilon^2\tilde{E}_{12}(\tau,t)+\varepsilon^3\tilde{E}_{13}(\tau,t)+\cdots\ , \tag{4.1a}$$

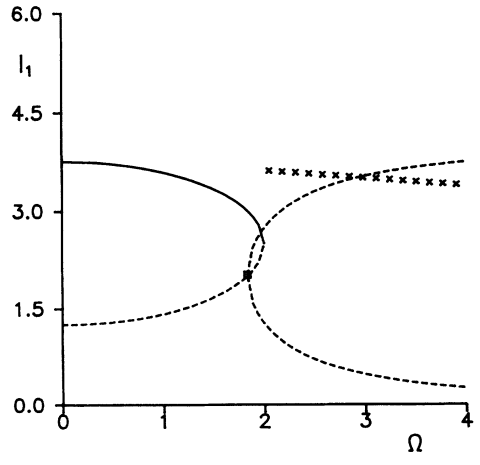

FIG. 1. Intensities I_1 of steady-state solutions (dashed and solid lines) and maxima of the periodic solutions (crosses) vs cavity-rotation rate Ω for dissipative coupling ($a=4$, $V=2$, $\xi=0.6$). Solid lines and crosses indicate stable solutions, dashed lines indicate unstable solutions. The square marks a steady bifurcation.

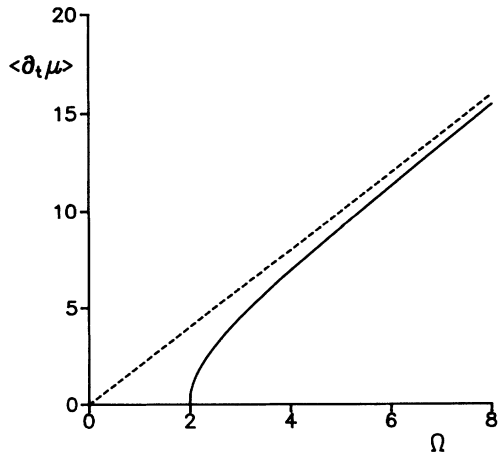

FIG. 2. Beat frequency vs cavity-rotation rate Ω for dissipative coupling ($V=2$, $\xi=0.6$). The beat frequency is independent of the pump parameter a. The dashed line corresponds to the ideal case ($\langle\partial_t\mu\rangle=2\Omega$).

$$\tilde{E}_2(\tau,t)=\varepsilon\tilde{E}_{21}(\tau,t)+\varepsilon^2\tilde{E}_{22}(\tau,t)+\varepsilon^3\tilde{E}_{23}(\tau,t)+\cdots , \tag{4.1b}$$

where $\tau=\varepsilon^2 t$ and ε is defined through $a=a_2\varepsilon^2$, $a_2=\pm 1$. The solution (4.1) can bifurcate either subcritically (i.e., $a<0$) or supercritically (i.e., $a>0$). This is determined by the following calculation, together with the stability property of the emerging solution (4.1). Substituting the expansions (4.1) into Eqs. (2.1) and collecting all terms of $\mathcal{O}(\varepsilon)$ gives

$$\partial_t\tilde{E}_{11}=-iV\tilde{E}_{21}-i\Omega\tilde{E}_{11} , \tag{4.2a}$$

$$\partial_t\tilde{E}_{21}=-iV\tilde{E}_{11}+i\Omega\tilde{E}_{21} . \tag{4.2b}$$

The solution of this system of linear equations is

$$\begin{bmatrix}\tilde{E}_{11}\\ \tilde{E}_{21}\end{bmatrix}=\tilde{A}_1(\tau)\begin{bmatrix}1\\ -\Delta_+\end{bmatrix}e^{i\omega_0 t}+\tilde{A}_2(\tau)\begin{bmatrix}1\\ \Delta_-\end{bmatrix}e^{-i\omega_0 t} , \tag{4.3}$$

with $\omega_0=(\Omega^2+V^2)^{1/2}$ and $\Delta_\pm=(\omega_0\pm\Omega)/V$. The slowly varying amplitudes $\tilde{A}_j$ are determined by an analysis of the $\mathcal{O}(\varepsilon^3)$ equations which are

$$\partial_t\tilde{E}_{13}=-iV\tilde{E}_{23}-i\Omega\tilde{E}_{13}+(a_2-|\tilde{E}_{11}|^2-\xi|\tilde{E}_{21}|^2)\tilde{E}_{11}-\partial_\tau\tilde{E}_{11} , \tag{4.4a}$$

$$\partial_t\tilde{E}_{23}=-iV\tilde{E}_{13}+i\Omega\tilde{E}_{23}+(a_2-|\tilde{E}_{21}|^2-\xi|\tilde{E}_{11}|^2)\tilde{E}_{21}-\partial_\tau\tilde{E}_{21} . \tag{4.4b}$$

Substituting the solution (4.3) into Eqs. (4.4) there appear inhomogeneous terms oscillating with frequencies $\pm\omega_0$, which are also the eigenfrequencies of the homogeneous equations. Such a situation leads to secular terms, i.e., diverging contributions. To avoid these divergencies, a solvability condition has to be used to cancel terms increasing without bound in time [17], which yields a system of coupled equations for the amplitudes $\tilde{A}_j$:

$$2\omega_0V\Delta_+\partial_\tau A_1=\{a_2 2\omega_0V\Delta_+-2\Delta_+^2[2\omega_0^2-(1-\xi)V^2]A_1^2-4[(1-\xi)V^2+2\omega_0^2\xi]A_2^2\}A_1 , \tag{4.5a}$$

$$2\omega_0V\Delta_-\partial_\tau A_2=\{a_2 2\omega_0V\Delta_--4[(1-\xi)V^2+2\omega_0^2\xi]A_1^2-2\Delta_-^2[2\omega_0^2-(1-\xi)V^2]A_2^2\}A_2 , \tag{4.5b}$$

where we set $\tilde{A}_j=A_j e^{i\alpha_j}$. The equations for the phases α_j are trivial. To proceed further, the steady-state solutions of Eqs. (4.5) are determined. There are two degenerate solutions:

$$A_{10}^2=a_2\frac{\omega_0V^2}{(\omega_0+\Omega)[2\omega_0^2-(1-\xi)V^2]},\quad A_{20}=0 , \tag{4.6a}$$

$$A_{10}=0,\quad A_{20}^2=a_2\frac{\omega_0V^2}{(\omega_0-\Omega)[2\omega_0^2-(1-\xi)V^2]} . \tag{4.6b}$$

The condition $A_{j0}^2>0$ imposes $a_2=1$. Substituting these solutions for the amplitude into Eqs. (4.3) yields a harmonically oscillating solution with constant intensity. We refer to this solution as a steady state. If $A_j\neq 0$ for $j=1,2$, the following equations for the amplitudes can be derived:

$$(V^2-2\Omega^2)\{-a_2\omega_0V\Delta_-+[(1-\xi)V^2+2(1+\xi)\omega_0^2]A_1^2\}=0 , \tag{4.7a}$$

$$(V^2-2\Omega^2)\{-a_2\omega_0V\Delta_++[(1-\xi)V^2+2(1+\xi)\omega_0^2]A_2^2\}=0 . \tag{4.7b}$$

Note that at $\Omega=V/\sqrt{2}$ the amplitudes are undetermined. Otherwise they are given by

$$A_{10}^2=\frac{\omega_0(\omega_0-\Omega)}{(1-\xi)V^2+2(1+\xi)\omega_0^2} , \tag{4.8a}$$

$$A_{20}^2=\frac{\omega_0(\omega_0+\Omega)}{(1-\xi)V^2+2(1+\xi)\omega_0^2} , \tag{4.8b}$$

where the solutions exist only for $a_2=1$. Thus we found two branches of solutions bifurcating at $a=0$. The phases α_j are in both cases undetermined.

To determine the stability of the solutions (4.6) and (4.8) we substitute $A_j=A_{j0}+\delta A_j$ into the amplitude equations (4.5) and linearize with respect to δA_j. For the steady-state solution (4.6a) the linearized problem is

$$2\omega_0V\Delta_+\partial_\tau\delta A_1=-4\Delta_+^2[2\omega_0^2-(1-\xi)V^2]A_{10}^2\delta A_1 , \tag{4.9a}$$

$$2\omega_0V\Delta_-\partial_\tau\delta A_2=\{2\omega_0V\Delta_--4[(1-\xi)V^2+2\omega_0^2\xi]A_{10}^2\}\delta A_2 . \tag{4.9b}$$

Substituting Eq. (4.6a) for A_{10}^2 the roots of the characteristic equation are

$$\lambda_1=-2,\quad \lambda_2=-\frac{(1-\xi)(V^2-2\Omega^2)}{(1+\xi)V^2+2\Omega^2} . \tag{4.10}$$

The solution (4.6b) yields the same eigenvalues. In terms of Ω, the branch of steady-state solutions becomes unstable via a steady bifurcation at $\Omega_c=V/\sqrt{2}$. For Eqs. (4.8), representing the branch of periodic solutions, the linearized problem is

$$2\omega_0V\Delta_+\partial_\tau\delta A_1=-4\Delta_+^2[2\omega_0^2-(1-\xi)V^2]A_{10}^2\delta A_1-8[(1-\xi)V^2+2\omega_0^2\xi]A_{10}A_{20}\delta A_2 , \tag{4.11a}$$

$$2\omega_0V\Delta_-\partial_\tau\delta A_2=-8[(1-\xi)V^2+2\omega_0^2\xi]A_{10}A_{20}\delta A_1-4\Delta_-^2[2\omega_0^2-(1-\xi)V^2]A_{20}^2\delta A_2 . \tag{4.11b}$$

Substituting Eqs. (4.8) for A_{10} and A_{20}, the roots of the characteristic equation are found to be

$$\lambda_1=-2,\quad \lambda_2=\frac{2(1-\xi)(V^2-2\Omega^2)}{(1-\xi)V^2+2(1+\xi)\omega_0^2} . \tag{4.12}$$

Thus in terms of Ω the branch of periodic solutions becomes stable via a steady bifurcation at $\Omega_c = V/\sqrt{2}$. The bifurcations on the branches (4.6) and (4.8) occur at the same value of $\Omega = \Omega_c$. There is a vertical branch of periodic solutions connecting these bifurcation points, due to the indetermination of A_j from Eqs. (4.7).

It turns out that for $\xi = 1$ the solution (4.3) is an exact solution of Eqs. (2.1), which is marginally stable since $\lambda_1 = -2$ and $\lambda_2 = 0$. This means that the expansions (4.1) are limited to the first term.

B. Steady-state solutions and their stability

As pointed out before, at $a = 0$ there is a Hopf bifurcation on the branch of trivial solutions where a branch of solutions with constant intensity, referred to as steady-state solutions, and a branch of periodic solutions emerge. To examine the steady-state solutions away from $a \ll 1$ the following transformation is introduced:

$$x = 2E_1E_2\cos(\mu), \quad y = 2E_1E_2\sin(\mu) , \qquad z = E_1^2 - E_2^2, \quad r = E_1^2 + E_2^2 , \tag{4.13}$$

where $x^2+y^2+z^2 = r^2$. With these variables Eqs. (2.3) are

$$\partial_t x = [2a - (1+\xi)r]x - 2\Omega y , \tag{4.14a}$$

$$\partial_t y = [2a - (1+\xi)r]y - 2Vz + 2\Omega x , \tag{4.14b}$$

$$\partial_t z = 2(a - r)z + 2Vy , \tag{4.14c}$$

$$\partial_t r = [2a - (1+\xi)r]r - (1-\xi)z^2 . \tag{4.14d}$$

These equations present a useful symmetry property: if the set $\{x(t), y(t), z(t), r(t)\}$ is a solution, then the set $\{-x(t), -y(t), -z(t), r(t)\}$ is also a solution. Solutions which are invariant under this transformation are referred to as symmetric solutions. Due to the symmetry of Eqs. (4.14), steady-state solutions are degenerate. For the special case $\xi = 1$, it is straightforward to get the general solution of Eqs. (4.14) (see Appendix B).

The frequency derived from Eqs. (2.4) is given by

$$\omega = \Omega \frac{r}{z} . \tag{4.15}$$

Under steady-state conditions Eqs. (4.14a) and (4.14b) can be written as

$$[2a - (1+\xi)r]x - 2\Omega y = 0 , \tag{4.16a}$$

$$2\Omega(a - r)x + \{[2a - (1+\xi)r](a - r) + 2V^2\}y = 0 . \tag{4.16b}$$

In order to have a nontrivial solution for x and y, the determinant of the coefficients must vanish, which yields an equation for $r' = 2a - (1+\xi)r$:

$$r'^3 - a(1-\xi)r'^2 + [4\Omega^2 + 2V^2(1+\xi)]r' - a(1-\xi)4\Omega^2 = 0 . \tag{4.17}$$

We first discuss the solution of this equation as a function of the pump parameter a. Solving Eq. (4.17) for a gives

$$a(r') = \frac{r'[r'^2 + 4\Omega^2 + 2V^2(1+\xi)]}{(1-\xi)(r'^2 + 4\Omega^2)} . \tag{4.18}$$

Since r must be positive, it follows that $a > r'/2$ which can be shown to be fulfilled by Eq. (4.18). As $r' \to \infty$ we have $r' \propto a(1-\xi)$ and therefore $r \propto a$. The local extrema of $a(r')$ correspond to the limit points of $r'(a)$. $a(r')$ has local extrema at

$$r_0'^2 = V^2(1+\xi) - 4\Omega^2 \pm \{V^2(1+\xi)[V^2(1+\xi) - 16\Omega^2]\}^{1/2} , \tag{4.19}$$

which is real for $16\Omega^2 < V^2(1+\xi)$. Hence Eq. (4.17) has three real solutions if this condition is verified and the solutions display a hysteresis domain when plotted versus the pump parameter a. In terms of a, the loci of the limit points in parameter space are given by

$$a_{01,2}^2(1-\xi)^2 = 9[V^2(1+\xi) - 4\Omega^2] + \frac{1}{8\Omega^2}[V^2(1+\xi) - 16\Omega^2]([V^2(1+\xi) - 16\Omega^2] \pm \{V^2(1+\xi)[V^2(1+\xi) - 16\Omega^2]\}^{1/2}) . \tag{4.20}$$

The two limit points coincide at $16\Omega^2 = V^2(1+\xi)$ where $a_{01}^2 = a_{02}^2 = 27V^2(1+\xi)/[4(1-\xi)^2]$. For $16\Omega^2 < V^2(1+\xi)$ it is straightforward to show that $a_{0j}^2 > 27V^2(1+\xi)/[4(1-\xi)^2]$. For $\Omega \to 0$ we have $a_{01}^2 \to \infty$ and $a_{02}^2 \to 8V^2(1+\xi)/(1-\xi)^2$ (see the solid lines in Fig. 3). In the limit $\xi \to 1$, the two limit points recede to infinity.

We now discuss the branch of steady-state solutions as a function of Ω^2 by solving Eq. (4.17) for this parameter:

$$\Omega^2(r') = -\frac{r'\{[r' - a(1-\xi)]r' + 2V^2(1+\xi)\}}{4[r' - a(1-\xi)]} . \tag{4.21}$$

This function is negative for $r' < 0$ and for $r' > a(1-\xi)$, i.e., r' is confined to the interval $(0, a(1-\xi))$. In terms of r, this condition is $a < r < 2a/(1+\xi)$. In the interval $(0, a(1-\xi))$ the function given by Eq. (4.21) has zeros at

$$r_{1,2}' = \frac{a(1-\xi)}{2} \pm \tfrac{1}{2}[a^2(1-\xi)^2 - 8V^2(1+\xi)]^{1/2} , \tag{4.22}$$

which is real for $a^2(1-\xi)^2 > 8V^2(1+\xi)$. Since, in the interval (r_1', r_2'), $\Omega^2(r')$ is negative, $r'(\Omega)$ has a gap at $\Omega = 0$ in this case (Fig. 4). The condition for multiple solutions is $a^2(1-\xi)^2 > 27V^2(1+\xi)/4$. If this condition is not fulfilled, $r'(\Omega)$ has no limit points, since

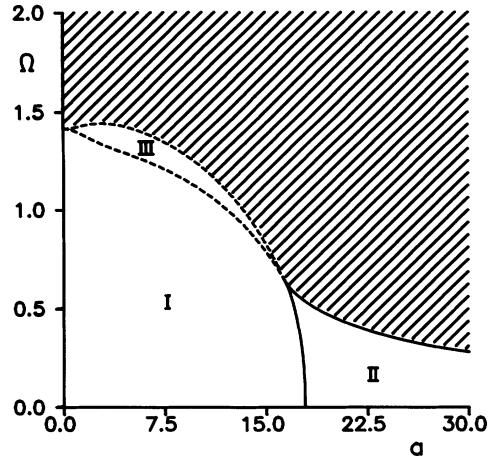

FIG. 3. Loci of bifurcation points (dashed lines) and limit points (solid lines) in the parameter plane (a,Ω) for conservative coupling ($V=2$, $\xi=0.6$). The upper dashed line corresponds to bifurcation points on branches of periodic solutions. The lower dashed line corresponds to Hopf bifurcation points on branches of steady-state solutions. In the hatched region the laser gyroscope is unlocked. In regions I and II it is locked. For a smaller than the value corresponding to the cusp formed by the two solid lines, the boundary between locked and unlocked domains lies in region III.

$a_{0j}^2(1-\xi)^2>27V^2(1+\xi)/4$ as pointed out before. Finally, if we expand r as $r_0+ar_1+\cdots$ with $a\ll 1$, we obtain from Eq. (4.17)

$$r_0=0,\quad r_1=\frac{2(\Omega^2+V^2)}{2\Omega^2+V^2(1+\xi)}\ . \tag{4.23}$$

which is compatible with the result

$$|\tilde{E}_{11}|^2+|\tilde{E}_{12}|^2=(1+\Delta_+^2)|\tilde{A}_1|^2=\frac{2(\Omega^2+V^2)}{2\Omega^2+V^2(1+\xi)}\ , \tag{4.24}$$

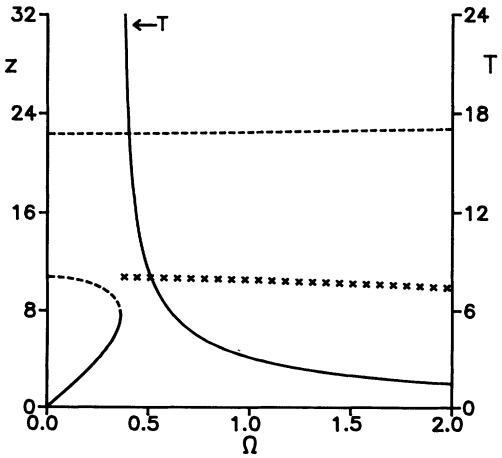

FIG. 4. Intensity differences z of steady-state solutions, maxima of the periodic solutions, and their period T vs cavity-rotation rate Ω for conservative coupling ($a=24$, $V=2$, $\xi=0.6$). Same conventions as in Fig. 1 for lines and crosses.

derived directly from Eqs. (4.3) and (4.6) in the small-a limit.

The expansion for $a\ll 1$ yields that the steady-state solutions bifurcate stably at $a=0$ for $\Omega<\Omega_c$ and unstably for $\Omega>\Omega_c$. As a increases, the unstable branch of steady-state solutions remains unstable. For $\Omega_c>\Omega>V\sqrt{1+\xi}/4$, the branch of stable steady-state solutions is destabilized via a Hopf bifurcation (Fig. 5). For the values of V and ξ chosen in Fig. 5, it can be shown graphically that there is only one Hopf bifurcation on the steady-state branch. In the case of multiple solutions (hysteresis domain), i.e., if $\Omega<V\sqrt{1+\xi}/4$, the branch of steady-state solutions is destabilized at the limit point a_{01} (Fig. 6). We have observed that, in general, it is not restabilized at the other limit point, i.e., at a_{02}; an example of this situation is displayed in Fig. 6. The exception is, however, a very small domain of values of Ω just below $V\sqrt{1+\xi}/4$. In this case the branch of steady-state solutions is stable from the other limit point up to a Hopf bifurcation.

Discussing the stability of the steady-state solutions in terms of Ω, the behavior is similar (compare the lower dashed line in Fig. 3). As Ω increases, the branch of steady-state solutions is destabilized via a Hopf bifurcation for $0<a<3V\sqrt{3(1+\xi)}/[2(1-\xi)]$ as shown in Fig. 7. This happens at $\Omega=\Omega_c$ for $a\ll 1$. Otherwise the destabilization occurs at a limit point (Fig. 4).

C. Periodic solutions and their stability

The periodic solutions obtained from the small-a expansion, i.e., Eq. (4.3) with A_j given by Eqs. (4.8), can be written in terms of the variables $\{x,y,z,r\}$ as

$$x=-4a\frac{\Omega}{V}A_1A_2\cos(2\omega_0t+\alpha_1-\alpha_2)\ , \tag{4.25a}$$

$$y=-4a\frac{\omega_0}{V}A_1A_2\sin(2\omega_0t+\alpha_1-\alpha_2)\ , \tag{4.25b}$$

$$z=4aA_1A_2\cos(2\omega_0t+\alpha_1-\alpha_2)\ , \tag{4.25c}$$

$$r=2a(A_1^2+A_2^2)\ . \tag{4.25d}$$

These solutions are symmetric as can be seen from the change of t into $t+\pi/2\omega_0$. In terms of the variables E_1, E_2, and μ, the symmetry of these solutions takes the form $E_2(t)=E_1(t+T/2)$ and $\mu(t+T/2)=\mu(t)+\pi$ where T is the period. It was proved in Sec. IV A that these solutions bifurcate unstably at $a=0$ for $\Omega<\Omega_c$ and stably for $\Omega>\Omega_c$.

For $\Omega>\Omega_c$, it was found numerically that for sufficiently large Ω, the branch of symmetric periodic solutions remains stable. For smaller values of Ω, this branch has a finite domain of instability, beginning and terminating with symmetry-breaking bifurcations. This pair of bifurcations is connected by two branches of stable asymmetric periodic solutions. These two asymmetric branches of solutions are related by the transformation $\{x,y,z,r\}\rightarrow\{-x,-y,-z,r\}$. In the original representation of Eqs. (2.1), the asymmetric solutions correspond to quasiperiodic solutions.

For $\Omega_c>\Omega>V\sqrt{1+\xi}/4$ the branch of unstable sym-

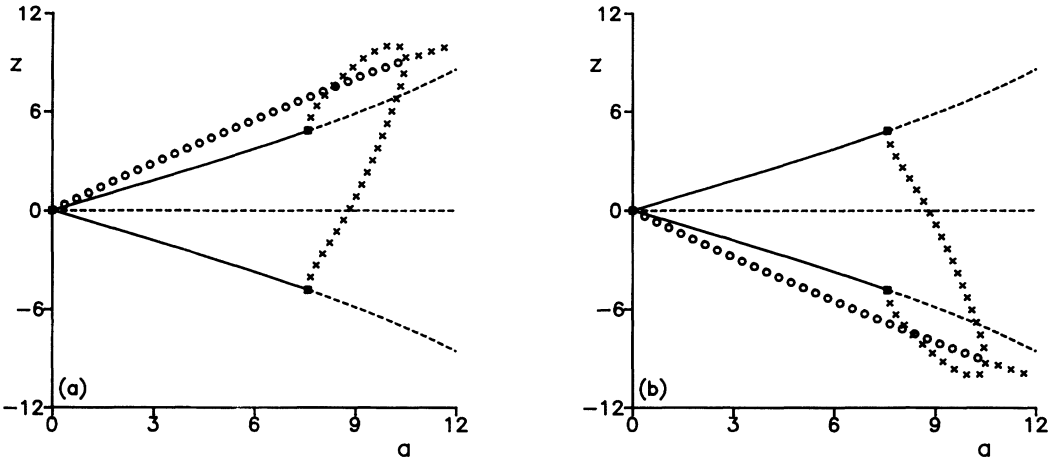

FIG. 5. Intensity differences z of steady-state solutions and (a) maxima of the periodic solutions, (b) minima of the periodic solutions, vs pump parameter a for conservative coupling ($\Omega=1.2$, $V=2$, $\xi=0.6$). Same conventions as in Fig. 1 for lines and crosses. Circles indicate unstable periodic solutions and black squares mark Hopf bifurcations.

metric periodic solutions becomes stable at a very special bifurcation point, which is both a symmetry-breaking bifurcation and a limit point for the branch of asymmetric solutions which emerge from the Hopf bifurcation on the branch of steady-state solutions. This is clearly displayed in Fig. 5.

In Fig. 3 we have summarized the stability results for the conservative case in the (a,Ω) plane. The upper dashed line is the locus of symmetry-breaking bifurcations that appear on the branch of symmetric periodic solutions. All the other lines refer to instabilities of steady-state branches and have been documented in previous sections. A homoclinic point occurs at $(a,\Omega)=(3V\sqrt{3(1+\xi)}/[2(1-\xi)], V\sqrt{1+\xi}/4)$ as far as numerical simulations can be trusted. From this point, a cusp emerges, which is formed by the two solid lines in Fig. 3 whose equations are given by Eq. (4.20). For $\Omega < V\sqrt{1+\xi}/4$, the bifurcation diagram is drastically modified, as shown by comparing Figs. 5 and 6. We first notice that the steady state becomes bistable. The main modification, however, is the disappearance of the symmetry-breaking bifurcation on the branch of periodic solutions which now splits up in two branches. The branch of periodic solutions emerging from the origin is still unstable. However, it ends abruptly with a homoclinic point which has the same coordinate as the limit point a_{02} [defined by Eq. (4.20)]. Likewise, at the other limit point, a_{01}, a new branch of periodic solutions emerges from a homoclinic point. This second branch, however, is stable. This situation is similar to the case of dissipative coupling.

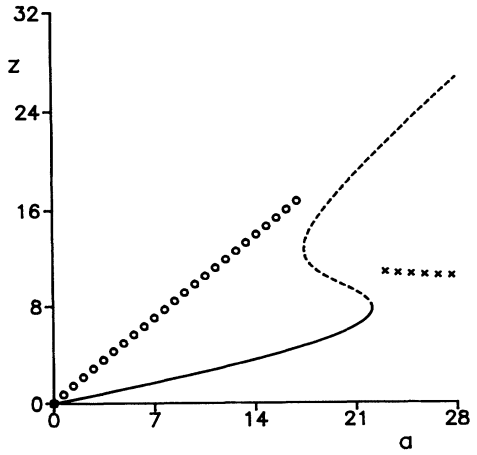

FIG. 6. Intensity differences z of steady-state solutions and maxima of the periodic solutions vs pump parameter a for conservative coupling ($\Omega=0.4$, $V=2$, $\xi=0.6$). Same graphical conventions as in Fig. 5.

Note that if we scan the (a,Ω) plane vertically, keeping a constant but less than the cusp value $3V\sqrt{3(1+\xi)}/[2(1-\xi)]$, the symmetry-breaking bifurcation always occurs (Fig. 7). Thus the domain between the dashed lines in Fig. 3 is characterized by the existence of stable asymmetric periodic solutions.

To sum up the results of the previous two sections, the laser behavior just above threshold is characterized by a constant output intensity for $\Omega < \Omega_c$, and by a periodically modulated output intensity for $\Omega > \Omega_c$. When a is further increased, a quasiperiodic regime appears for Ω verifying either $\Omega_c > \Omega > V\sqrt{1+\xi}/4$ or $\Omega - \Omega_c \ll 1$. For sufficiently large values of the pump parameter a, the output intensity is always periodically modulated. The domains in parameter space where the intensity is constant or quasiperiodically modulated decrease with the backscattering rate V. The limiting case $\xi=1$ is dealt with in Appendix B.

D. Locking behavior

For $a \ll 1$ an analytical expression for the beat frequency as a function of Ω can be derived using Eq. (4.3).

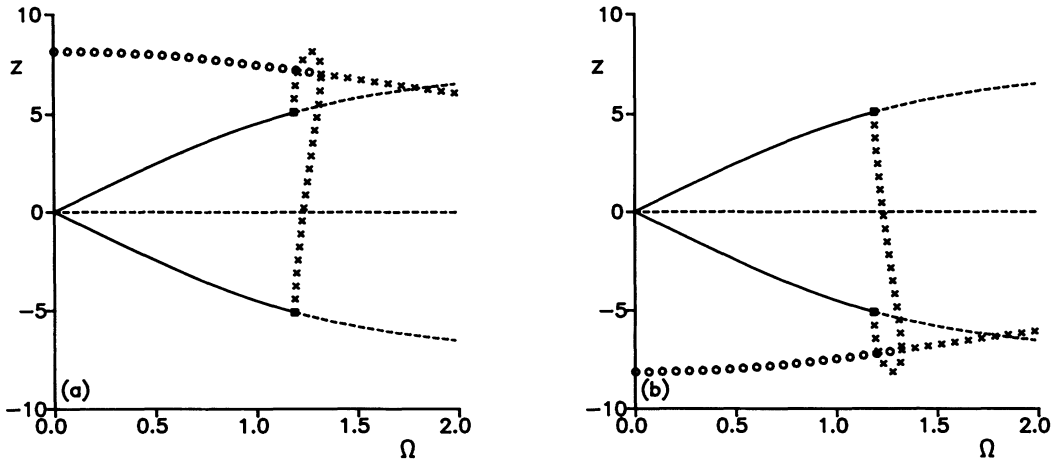

FIG. 7. Intensity differences z of steady-state solutions and (a) maxima of the periodic solutions, (b) minima of the periodic solutions, vs cavity-rotation rate Ω for conservative coupling ($a=8$, $V=2$, $\xi=0.6$). Same graphical conventions as in Fig. 5.

For $\Omega<\Omega_c$ the steady-state solution (4.6) is stable and $\langle\partial_t\mu\rangle=0$. For $\Omega>\Omega_c$ the periodic solution (4.8) is stable. With Eqs. (4.25a) and (4.25b) the phase difference μ is determined by

$$\tan(\mu)=\frac{\omega_0}{\Omega}\tan(2\omega_0 t+\alpha_1-\alpha_2)\ , \tag{4.26}$$

where $\tan(\mu)=y/x$ has been used. Calculating the integral (3.16) with Eq. (4.26) the beat frequency is

$$\langle\partial_t\mu\rangle=2\omega_0=2(\Omega^2+V^2)^{1/2}\ . \tag{4.27}$$

Thus for $a\ll 1$ the locking range is given by $\Omega_{L,c}=\Omega_c$. At $\Omega=\Omega_{L,c}$ the beat frequency as a function of Ω shows a gap. If the pump parameter a is relatively small the situation is similar to the passive-cavity case, since the passive-cavity eigenmodes are described by solution (4.3) with $\tilde{A}_j$ arbitrary constants and either $\tilde{A}_1=0$ or $\tilde{A}_2=0$. These eigenmodes have a frequency difference $2\omega_0$. Thus there is no locking in the passive-cavity case. The gain saturation or nonlinear coupling of the modes determines the competition between them and causes one of the eigenmodes to be extinguished for small Ω. Which one is extinguished depends on the difference in gain for the eigenmodes. Hence if the ring laser is set into rotation no beat frequency can be observed since only one of the eigenmodes is present; the laser gyroscope is locked since $\langle\partial_t\mu\rangle=0$. Increasing Ω the nonlinear coupling weakens and two-mode oscillations with a Sagnac-related beat frequency are observed. This explains the gap in the observed beat frequency.

For $a<3V\sqrt{3(1+\xi)}/[2(1-\xi)]$, the locking diagram, as displayed in Fig. 8, is similar to the case $a\ll 1$, except that the end of the locking range does not coincide with the Hopf bifurcation on the branch of steady-state solutions. A manifestation of this difference is seen in the time behavior of the phases. Somewhere on the branch of asymmetric periodic solutions, between the Hopf bifurcation on the branch of steady-state solutions and the symmetry-breaking bifurcation, the phase difference $\mu(t)$ displays a transition from a periodic to an increasing function. The occurrence of different behaviors of μ has also been reported by Chyba in [13], though without correlating it to the topological properties of the fields. Looking at the field portraits in the (x,y) plane, we observe that the orbit does not include the origin when μ is periodic, whereas it does include the origin otherwise (Fig. 9). This is in agreement with a recent analysis which relates in a similar way the topology of the field portrait to the behavior of the relative phase [18]. For a periodic function $\mu(t)$, the beat frequency defined by Eq. (3.16) is zero. In the other case, we have determined the beat frequency numerically by integrating Eqs. (4.14), calculating the period T of the orbits to get $\langle\partial_t\mu\rangle=\pi/T$. Hence, for increasing Ω, the laser gyroscope becomes unlocked and suddenly a beat frequency larger than expected in the absence of backscattering is observed.

For $a>3V\sqrt{3(1+\xi)}/[2(1-\xi)]$, the locking range ends at the limit point where the steady-state solution is

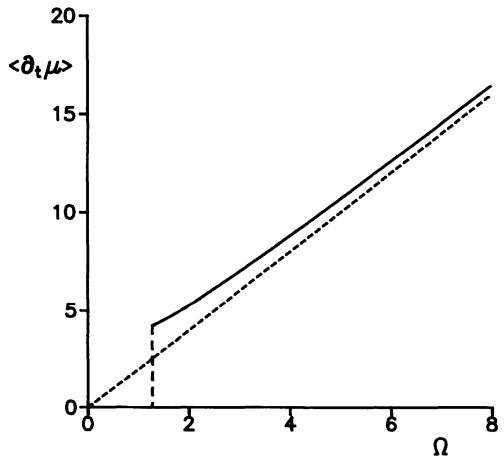

FIG. 8. Beat frequency vs cavity-rotation rate Ω for conservative coupling ($a=8$, $V=2$, $\xi=0.6$). The dashed line corresponds to the ideal case ($\langle\partial_t\mu\rangle=2\Omega$).

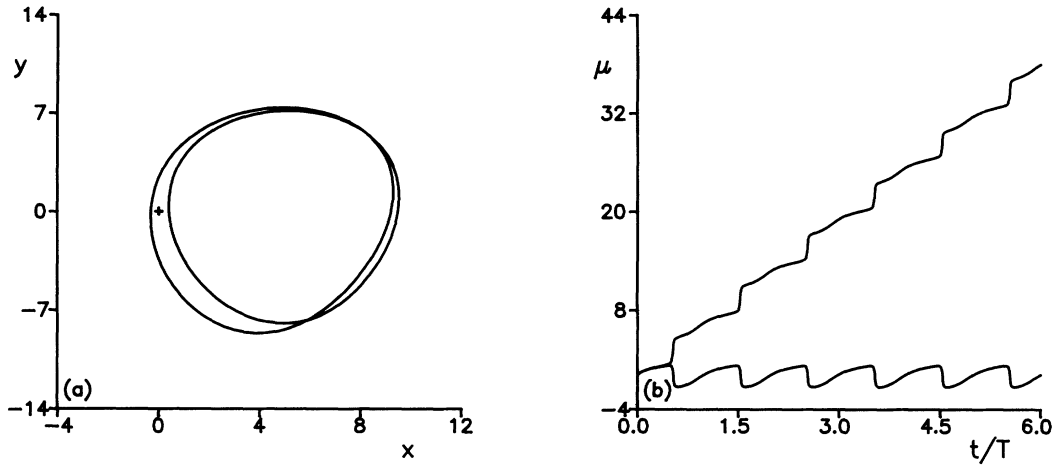

FIG. 9. (a) Field portraits in the plane (x,y) and (b) corresponding phase differences $\mu(t)$ for solutions on the branch of asymmetric periodic solutions of Fig. 7 for $\Omega=1.27$ [$\mu(t)$ periodic] and $\Omega=1.28$ [$\mu(t)$ increasing, the field portrait includes the origin marked by a cross].

destabilized. Since the branch of periodic solutions is approaching a homoclinic orbit at the limit point there is no gap in the locking diagram because a homoclinic orbit has infinite period (Fig. 10). Thus the laser gyroscope unlocks in a way similar to the dissipative coupling case. This is due to the fact that for large values of the pump parameter a the nonlinear coupling of the electric fields $\tilde{E}_1$ and $\tilde{E}_2$ due to gain saturation becomes larger than the strength of the conservative linear coupling. Since this nonlinear coupling is of dissipative character the gap in the locking diagram vanishes. This dissipative character can be seen by separating terms containing ξ in Eqs. (2.1) and writing them as

$$\partial_t\tilde{E}_1=(a-|\tilde{E}_1|^2-|\tilde{E}_2|^2)\tilde{E}_1-iV\tilde{E}_2 +(1-\xi)\tilde{E}_1\tilde{E}_2^*\tilde{E}_2-i\Omega\tilde{E}_1 , \quad (4.28a)$$

$$\partial_t\tilde{E}_2=(a-|\tilde{E}_1|^2-|\tilde{E}_2|^2)\tilde{E}_2-iV\tilde{E}_1 +(1-\xi)\tilde{E}_2\tilde{E}_1^*\tilde{E}_1+i\Omega\tilde{E}_2 . \quad (4.28b)$$

Considering the nature of the coupling terms $(1-\xi)\tilde{E}_1\tilde{E}_2^*\tilde{E}_2$ and $(1-\xi)\tilde{E}_2\tilde{E}_1^*\tilde{E}_1$, the resulting coupling matrix has a dissipative character. The critical value of the backscattering rate above which the backscattering is of conservative nature is given by $V_c=2a(1-\xi)/[3\sqrt{3(1+\xi)}]$. A similar case is discussed in [14]. For large values of Ω the nonlinear coupling is diminished and the system behaves as a truly conservatively locked laser gyroscope, i.e., the observed beat frequency approaches the ideal limit from above. The locking range decreases with increasing a (see upper solid line in Fig. 3).

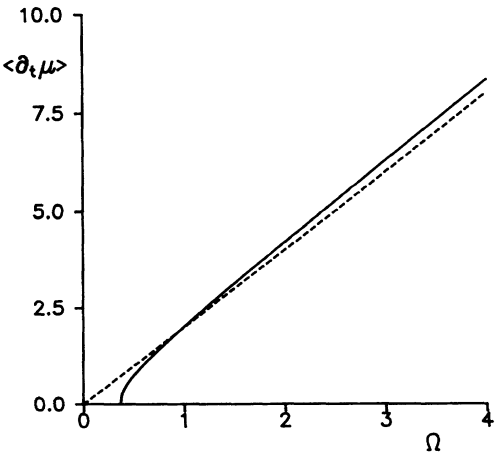

FIG. 10. Beat frequency vs cavity-rotation rate Ω for conservative coupling ($a=24$, $V=2$, $\xi=0.6$). The dashed line corresponds to the ideal case ($\langle\partial_t\mu\rangle=2\Omega$).

V. CONCLUSIONS

Discussing the stability of the solutions of the nonlinear Eqs. (2.1), we derived the locking behavior of the ring-laser gyroscope for the limiting cases of dissipative and conservative coupling. In the case of dissipative coupling, the locking range for the nonlinear problem is found to match the locking range neglecting the gain, losses, and saturation. Thus the locking behavior is determined by the characteristics of the passive-cavity case. However, the nonlinear coupling due to the gain saturation leads to intensities oscillating very anharmonically near the locking threshold $\Omega_{L,d}$. In the limit $\Omega\gg\Omega_{L,d}$ the intensities oscillate harmonically and are identical to the ones found in the case of a passive cavity.

In the conservative case, the locking behavior is completely determined by the nonlinear coupling, whereas for the dissipative case, it is solely determined by the strength of the backscattering. For sufficiently low pump, the passive-cavity eigenmodes can be used as a good approximation of the exact eigenmodes. However, in the case of an active cavity, the ring-laser gyroscope is

locked for $\Omega<\Omega_{L,c}$ as well. The locking diagram displays a gap at the locking threshold $\Omega_{L,c}$. As the pump increases, the passive-cavity eigenmodes are found to become less and less useful. The frequency jump vanishes. The locking diagram then resembles the one for dissipative coupling, as it starts with a zero beat frequency and increases as a function of Ω. However, at a certain rotation rate it exceeds the limit of an ideal laser gyroscope. This is in contrast to the case of pure dissipative coupling. In general, in the case of conservative coupling the locking range is always smaller than in the case of dissipative coupling and can be decreased further by increasing the pump parameter a (Fig. 3).

ACKNOWLEDGMENTS

This research was supported by the Interuniversity Attraction Pole program of the Belgian government. P.M. acknowledges partial support from the Fonds National de la Recherche Scientifique (Belgium). R.C.N., R.J.C.S., and J.P.W. acknowledge the Stichting voor Fundamenteel Onderzoek der Materie (FOM) and partial financial support from the Nederlandse Organisatie voor Wetenschappelijk Onderzoek (NWO).

APPENDIX A: STABILITY OF PERIODIC SOLUTIONS FOR DISSIPATIVE COUPLING

Substituting $E_{10}=E_{20}=E(t)$ and $\mu_0=\mu(t)$, where $E(t)$ and $\mu(t)$ are given by Eqs. (3.11) and (3.13), into Eq. (3.6) the system of linear equations with periodic coefficients governing the stability of the branch of periodic solutions is

$$\partial_t\begin{bmatrix}e_1\\e_2\\\mu_1\end{bmatrix}=\begin{bmatrix}a-(3+\xi)E^2(t) & -2\xi E^2(t)+V\cos[\mu(t)] & -VE(t)\sin[\mu(t)]\\ -2\xi E^2(t)+V\cos[\mu(t)] & a-(3+\xi)E^2(t) & -VE(t)\sin[\mu(t)]\\ 0 & 0 & -2V\cos[\mu(t)]\end{bmatrix}\begin{bmatrix}e_1\\e_2\\\mu_1\end{bmatrix}, \tag{A1}$$

where e_1, e_2, and μ_1 are small deviations from E_{10}, E_{20}, and μ_0. Adding and subtracting the first two of Eqs. (A1) we get the following system of equations:

$$\partial_t e_1'=\{a-3(1+\xi)E^2(t)+V\cos[\mu(t)]\}e_1' -2VE(t)\sin[\mu(t)]\mu_1 , \tag{A2a}$$

$$\partial_t e_2'=\{a-(3-\xi)E^2(t)-V\cos[\mu(t)]\}e_2' , \tag{A2b}$$

$$\partial_t\mu_1=-2V\cos[\mu(t)]\mu_1 . \tag{A2c}$$

Here $e_1'=e_1+e_2$ and $e_2'=e_1-e_2$. By means of Eqs. (A2) the set of fundamental solutions of Eqs. (A1) is obtained as

$$\begin{bmatrix}e_1\\e_2\\\mu_1\end{bmatrix}_1=\begin{bmatrix}\partial_t E(t)\\\partial_t E(t)\\\partial_t\mu(t)\end{bmatrix}, \tag{A3a}$$

$$\begin{bmatrix}e_1\\e_2\\\mu_1\end{bmatrix}_2=\begin{bmatrix}1\\1\\0\end{bmatrix}\exp\left[\int^t dt\{a-3(1+\xi)E^2(t)+V\cos[\mu(t)]\}\right], \tag{A3b}$$

$$\begin{bmatrix}e_1\\e_2\\\mu_1\end{bmatrix}_3=\begin{bmatrix}1\\-1\\0\end{bmatrix}\exp\left[\int^t dt\{a-(3-\xi)E^2(t)-V\cos[\mu(t)]\}\right]. \tag{A3c}$$

Solution (A3a) corresponds to the one with a Floquet multiplier of unity and is bounded, since the derivatives of $E(t)$ and $\mu(t)$ are bounded. To evaluate the integrals in Eqs. (A3b) and (A3c) we use Eq. (3.10a) to express he integral over I:

$$\int^t dt\, I(t)=\frac{1}{2(1+\xi)}\left\{2at-\ln I(t)+2V\int^t dt\cos[\mu(t)]\right\}. \tag{A4}$$

Substituting this expression the integrals in Eqs. (A3b) and (A3c) are

$$\int^t dt\{[a-3(1+\xi)I(t)+V\cos[\mu(t)]\}=-2at+\tfrac{3}{2}\ln I(t)-2V\int^t dt\cos[\mu(t)] , \tag{A5a}$$

$$\int^t dt\{a-(3-\xi)I(t)-V\cos[\mu(t)]\}=\frac{1}{1+\xi}\left\{-2(1-\xi)at+(3-\xi)\ln I(t)/2-4V\int^t dt\cos[\mu(t)]\right\}. \tag{A5b}$$

Apart from a constant the remaining integral in the right-hand side of Eqs. (A5a) and (A5b) is evaluated as

$$2V\int^t dt\,\cos[\mu(t)]=\ln\left[\frac{\Omega^2\{1+\tan^2[\mu(t)/2]\}}{1+\tan^2(\omega_0 t+\varphi_0)}\right], \tag{A6}$$

which is a bounded function of t. So is $\ln I(t)$. Hence the integrals in Eqs. (A3b) and (A3c) decrease exponentially as $\exp(-2at)$ and $\exp[-2(1-\xi)at/(1+\xi)]$, respectively. Note that $\xi<1$. Thus the solution given by Eqs. (3.11) and (3.13) is stable in the domain in parameter space where it exists.

APPENDIX B: THE CASE $\xi=1$ FOR CONSERVATIVE COUPLING

For conservative coupling, it is easy to deal with the well-known case $\xi=1$ (see [13]) using the variables (4.13). Equations (4.14) simplify considerably in this case:

$$\partial_t x=2(a-r)x-2\Omega y\ , \tag{B1a}$$

$$\partial_t y=2(a-r)y-2Vz+2\Omega x\ , \tag{B1b}$$

$$\partial_t z=2(a-r)z+2Vy\ , \tag{B1c}$$

$$\partial_t r=2(a-r)r\ . \tag{B1d}$$

The solution of Eq. (B1d) which is only dependent on r is

$$r(t)=\frac{2a}{2+C_0 e^{-2at}}\ , \tag{B2}$$

with C_0 an arbitrary constant. Introducing the transformation

$$x(t)=r(t)x'(t),\quad y(t)=r(t)y'(t)\ ,\qquad z(t)=r(t)z'(t)\ , \tag{B3}$$

where $x'^2(t)+y'^2(t)+z'^2(t)=1$, the following linear system of equations can be obtained:

$$\partial_t x'=-2\Omega y'\ , \tag{B4a}$$

$$\partial_t y'=-2Vz'+2\Omega x'\ , \tag{B4b}$$

$$\partial_t z'=2Vy'\ . \tag{B4c}$$

The solution of Eqs. (B4) is

$$\begin{bmatrix}x'\\y'\\z'\end{bmatrix}=C_1\begin{bmatrix}1\\0\\\Omega/V\end{bmatrix}+\begin{bmatrix}C_2\\-C_3\omega_0/\Omega\\-C_2 V/\Omega\end{bmatrix}\cos(2\omega_0 t)+\begin{bmatrix}C_3\\C_2\omega_0/\Omega\\-C_3 V/\Omega\end{bmatrix}\sin(2\omega_0 t)\ , \tag{B5}$$

with $\omega_0=(\Omega^2+V^2)^{1/2}$. From the condition $x'^2(t)+y'^2(t)+z'^2(t)=1$ there is a constraint on the constants C_1, C_2, and C_3:

$$\omega_0^2\left[\frac{1}{V^2}C_1^2+\frac{1}{\Omega^2}(C_2^2+C_3^2)\right]=1\ . \tag{B6}$$

In the long-time limit we have $r(t)=a$ and the solution is given by (B5), apart from a multiplication by a. Comparing the family of solutions (B5) with the result (4.25) from the expansion for $a\ll 1$, we see that for $\xi\to 1$ the solution

$$C_1=0,\quad C_2=-4\frac{\Omega}{V}A_1A_2\cos(\alpha_1-\alpha_2)\ ,\qquad C_3=4\frac{\Omega}{V}A_1A_2\sin(\alpha_1-\alpha_2) \tag{B7}$$

is selected, with $A_1A_2=V/4\omega_0$ from Eqs. (4.8). Similarly the steady-state solutions (4.6) correspond to $C_1=\pm V/\omega_0$ and $C_2=C_3=0$.

[1] F. Aronowitz and R. J. Collins, J. Appl. Phys. **41**, 130 (1970).

[2] F. Aronowitz, Appl. Opt. **1**, 405 (1972).

[3] L. N. Menegozzi and W. E. Lamb, Jr., Phys. Rev. A **8**, 2103 (1973).

[4] S. Stenholm, Acta Polytech. Scand. **138**, 165 (1983).

[5] H. A. Haus, H. Statz, and I. W. Smith, IEEE J. Quantum Electron. **QE-21**, 78 (1985).

[6] W. W. Chow, J. Gea-Banacloche, L. M. Pedrotti, V. E. Sanders, W. Schleich, and M. O. Scully, Rev. Mod. Phys. **57**, 61 (1985).

[7] J. P. Woerdman and R. J. C. Spreeuw, in *Analogies in Optics and Micro-Electronics,* edited by W. van Haeringen and D. Lenstra (Kluwer, Dordrecht, 1990), pp. 135–150.

[8] D. Kühlke, Acta Phys. Pol. A **61**, 547 (1982).

[9] W. R. Christian and L. Mandel, Phys. Rev. A **34**, 3932 (1986); W. R. Christian, E. C. Gage, and L. Mandel, Opt. Lett. **12**, 328 (1987); W. R. Christian and L. Mandel, J. Opt. Soc. Am. B **5**, 1406 (1988).

[10] W. R. Christian, T. H. Chyba, E. C. Gage, and L. Mandel, Opt. Commun. **66**, 238 (1988).

[11] N. B. Abraham and C. O. Weiss, Opt. Commun. **68**, 437 (1988).

[12] L. Pesquera, R. Blanco, and M. A. Rodrígues, Phys. Rev. A **39**, 5777 (1989); L. Pesquera and R. Blanco, Opt. Commun. **74**, 102 (1989).

[13] T. H. Chyba, Phys. Rev. A **40**, 6327 (1989); Opt. Commun. **76**, 395 (1990); in Laser Noise, edited by R. Roy [Proc. SPIE **1376**, 132 (1990)].

[14] R. Centeno Neelen, R. J. C. Spreeuw, E. R. Eliel, and J. P. Woerdman, J. Opt. Soc. Am. B **8**, 959 (1991).

[15] R. J. C. Spreeuw, R. Centeno Neelen, N. J. van Druten, E. R. Eliel, and J. P. Woerdman, Phys. Rev. A **42**, 4315 (1990).

[16] M. Sargent, M. O. Scully, and W. E. Lamb, Jr., *Laser Physics* (Addison-Wesley, Reading, MA, 1974).

[17] G. Iooss and D. D. Joseph, *Elementary Stability and Bifurcation Theory,* Undergraduate Texts in Mathematics (Springer-Verlag, Heidelberg, 1980).

[18] P. Mandel, P. Galatola, L. A. Lugiato, and Wang Kaige, Opt. Commun. **80**, 262 (1991).